Evidence for Nonbridged Coordination of *p*-Nitrophenyl Phosphate to the Dinuclear Fe(III)−M(II) Center in Bovine Spleen Purple Acid Phosphatase during Enzymatic Turnover

Maarten Merkx, Martijn W. H. Pinkse, and Bruce A. Averill*

E.C. Slater Institute, Biocentrum Amsterdam, University of Amsterdam, Plantage Muidergracht 12, 1018 TV Amsterdam, The Netherlands

Received February 24, 1999; Revised Manuscript Received June 7, 1999

ABSTRACT: The pH dependence of the catalytic parameters k_{cat} and K_M has been determined for the Fe(III)Fe(II)- and Fe(III)Zn(II)-forms of bovine spleen purple acid phosphatase (BSPAP). The parameter k_{cat} was found to be maximal at pH 6.3, and a pK_a of 5.4−5.5 was obtained for the acidic limb of the k_{cat} vs pH profile. Two different EPR spectra were detected for the phosphate complex of the mixed-valent diiron enzyme; their relative amounts depended on the pH, with an apparent pK_a of 6. The EPR spectra of Fe(III)Fe(II)−BSPAP·PO_4 and Fe(III)Zn(II)−BSPAP·PO_4 at pH 5.0 are similar to those previously reported for Fe(III)Fe(II)−Uf·PO_4 and Fe(III)Zn(II)−Uf·PO_4 complexes at pH 5.0. At higher pH, a new Fe(III)Fe(II)−BSPAP·PO_4 species is formed, with apparent *g*-values of 1.94, 1.71, and 1.50. The EPR spectrum of Fe(III)Zn(II)−BSPAP does not show significant changes upon addition of phosphate up to 30 mM at pH 6.5, suggesting that phosphate binds only to the spectroscopically silent Zn(II). To determine whether the phosphate complexes were good structural models for the enzyme substrate complexes, these complexes were studied using rapid-freeze EPR and stopped-flow optical spectroscopy. The stopped-flow studies showed the absence of burst kinetics at pH 7.0, which indicates that substrate hydrolysis is rate limiting, rather than phosphate release. The EPR spectrum of Fe(III)Fe(II)−BSPAP·*p*-NPP is similar, but not identical, to that of the corresponding phosphate complex, both at pH 5 and pH 6.5. We propose that both phosphate and *p*-NPP bridge the two metal ions at low pH. At higher pH where the enzyme is optimally active, we propose that hydroxide competes with phosphate and *p*-NPP for coordination to Fe(III) and that both phosphate and *p*-NPP coordinate only to the divalent metal ion.

The purple acid phosphatases (PAPs)[1] belong to a growing family of hydrolases that employ a di- or trinuclear metal center in their active sites (*1*, *2*). While most of these enzymes contain divalent metal ions, such as Zn^{2+}, Mg^{2+}, Mn^{2+}, or Co^{2+}, the PAPs contain an $Fe^{3+}Fe^{2+}$ or $Fe^{3+}Zn^{2+}$ center (*3*). All PAPs from mammalian sources contain an antiferromagnetically coupled FeFe metal center, although bovine spleen purple acid phosphatase (BSPAP) has recently been shown to contain a small "impurity" with an $Fe^{3+}Zn^{2+}$ center (*4*). Uteroferrin (Uf) and BSPAP are two mammalian PAPs that have extensively been studied by a variety of spectroscopic methods, including EPR, Mössbauer, EXAFS, resonance Raman, and paramagnetically shifted ^{1}H NMR spectroscopy (*3*). These studies showed that the distinct purple color of the enzyme is due to the coordination of a tyrosinate ligand to the ferric iron. They also provided important insights into the structure of complexes of inhibitory oxoanions, such as phosphate, arsenate, molybdate, vanadate, and tungstate (*5*−*16*). The best studied plant purple acid phosphatase is that isolated from red kidney beans. Kidney bean PAP (KBPAP) contains an Fe(III)Zn(II) metal center and is the only PAP for which an X-ray structure has been reported (*17*, *18*). Although there is little overall sequence homology between KBPAP and the mammalian enzymes, all the metal-coordinating amino acids and some of the amino acids in the proximity of the dinuclear metal center are conserved among all PAPs, suggesting a similar active site structure (*3*, *19*). Also, one of the irons in BSPAP and Uf can be replaced by zinc without drastic effects on the phosphatase activity (*4*, *10*, *20*−*22*). Conversely, the zinc in KBPAP can be substituted by iron, again without major

* To whom correspondence should be addressed. Telephone: 31-20-5255045. Fax: 31-20-5255124. E-mail: BAA@chem.uva.nl.

[1] Abbreviations: BSA, bovine serum albumin; BSPAP, bovine spleen purple acid phosphatase; CD, circular dichroism; ESEEM, electron-spin−echo envelope modulation; ENDOR, electron−nuclear double resonance spectroscopy; EPR, electron paramagnetic resonance; EXAFS, extended X-ray absorption fine structure; FeFe−BSPAP, BSPAP with iron at the ferric and ferrous sites; FeFe−BSPAP·PO_4, FeFe−BSPAP complexed with phosphate; FeFe−BSPAP·*p*-NPP, FeFe−BSPAP complexed with *p*-NPP; FeFe−Uf, Uf with iron at the ferric and ferrous sites; FeFe−Uf·PO_4, FeFe−Uf complexed with phosphate; FeZn−BSPAP, BSPAP with iron at the ferric site and zinc at the ferrous site; FeZn−BSPAP·PO_4, FeZn−BSPAP complexed with phosphate; FeZn−Uf, Uf with iron at the ferric site and zinc at the ferrous site; FeZn−Uf·PO_4, FeZn−Uf complexed with phosphate; HEPES, N-[2-hydroxyethyl]piperazine-N′-[2-ethanesulfonic acid]; KBPAP, purple acid phosphatase of red kidney beans; MCD, magnetic circular dichroism; MES, 2-[N-morpholino]ethanesulfonic acid; MOPS, 3-[N-morpholino]propanesulfonic acid; PAP, purple acid phosphatase; *p*-NP, *p*-nitrophenol; *p*-NPP, disodium salt of *p*-nitrophenyl phosphate; PP, protein phosphatase; PP1, protein phosphatase 1; PP2B, protein phosphatase 2B; $P_{1/2}$, microwave power at half saturation; Uf, uteroferrin.

10.1021/bi9904454 CCC: $18.00
Published on Web 07/13/1999

effects on catalysis (*23*−*25*). A sequence motif that incorporates most of the conserved amino acids of PAP is found in a much larger group of phosphohydrolases, among which are exonucleases, 5′-nucleotidases, diadenosinetetraphosphatases and Ser/Thr specific protein phosphatases (*18*, *26*, *27*). X-ray structure determinations of two Ser/Thr specific protein phosphatases, PP1 (*28*, *29*) and PP2B (calcineurin) (*30*, *31*), have revealed a dinuclear metal center resembling that of the PAPs, except for the tyrosinate ligand to the Fe^{3+} that gives the PAPs their characteristic purple color.

PAPs are optimally active under weakly acidic conditions, a feature which has been attributed to the ability of the strong Lewis acid Fe^{3+} to generate the nucleophilic hydroxide ion even under acidic conditions. The mammalian enzymes are catalytically active in the mixed-valent Fe(III)Fe(II)-state, and totally inactive in the Fe(III)Fe(III) oxidation state (*4*). Initially, our group reported certain phenomena (burst kinetics at pH 9, transphosphorylation) that indicated the existence of a covalent phosphoenzyme intermediate during BSPAP catalysis (*32*). However, subsequent studies showed that these phenomena were probably due to experimental artifacts (*33*, *34*). Moreover, Mueller et al. showed that BSPAP catalyzes the hydrolysis of phosphate esters with net inversion of the stereoconfiguration around phosphorus (*35*). This important result supports a mechanism in which the phosphate ester is directly attacked by water and rules out a phosphoenzyme intermediate. However, some important mechanistic questions remain unanswered. It is not known whether the phosphate ester binds to both metal ions in a bridging mode (like phosphate in the structurally characterized PAP and PPs) or whether it coordinates only to the divalent metal ion. The nature of the attacking water/hydroxide nucleophile is another subject of debate. Possible candidates are the hydroxide bridging the two metals, the hydroxide bound terminally to the Fe^{3+}, and a water/hydroxide in the second coordination sphere of the Fe^{3+} (*7*, *11*, *18*, *36*, *37*).

In the absence of a good nonhydrolyzable substrate analogue, phosphate has been assumed to mimic the binding mode of the phosphate ester substrate, although it is actually one of the products of the reaction. Phosphate has been reported to be a competitive (Uf, pH 5) (*5*, *38*) or mixed-type inhibitor (BSPAP, pH 6) (*12*) with an affinity similar to that for substrate. Several spectroscopic studies have provided evidence that phosphate binds to both metal ions in a bridging coordination mode. David and Que showed that phosphate binds directly to the iron in Fe(III)Zn(II)−Uf at pH 5.0 using $P^{17}O_4$ and EPR (*10*). EXAFS studies on Fe(III)Zn(II)−Uf-PO_4 (pH 5) were also interpreted in terms of a bridging binding mode for phosphate (*7*). Finally, the X-ray structures of KBPAP complexed with phosphate and tungstate (pH 4.5) showed that both oxoanions bind to the dinuclear metal center in a bridging coordination mode (*18*). As indicated, these studies were performed at pH $\leq$5, as have been most other spectroscopic studies on PAPs. Other groups have reported pH-dependent changes in the spectral properties of the phosphate complex (*5*, *11*) and suggested a bridging phosphate coordination at low pH and end-on binding to the divalent metal ion (Fe^{2+} or Zn^{2+}) at higher pH (*11*). No systematic study has thus far been reported that correlates these pH dependent changes in spectral properties of the phosphate complex with the pH dependent changes in kinetics parameters, most importantly the pH dependence of k_{cat}.

Uf has been reported to have a rather narrow, bell-shaped pH-activity profile that is maximal at pH 5 (*36*, *39*). The optimal pH for BSPAP activity has been determined to be at pH 6−6.5 (*11*, *32*). All reports on the pH dependence of Uf and most studies on the pH dependence of BSPAP were carried out at a single, fixed substrate concentration, which can easily lead to the misinterpretation of the profiles if this substrate concentration is not saturating at all pH values. Only one previous study (on BSPAP) tried to separate the effect of pH on k_{cat} and K_M, but this work suffered from severely scattered datapoints (*32*).

In the present study, we examined the pH dependence of the kinetics parameters k_{cat} and k_{cat}/K_M, both for the native Fe(III)Fe(II)−BSPAP and for Fe(III)Zn(II)−BSPAP. Both forms show a bell-shaped dependence of k_{cat} on pH, with an acidic pK_a of ∼5.5 and a maximal k_{cat} at pH ∼6.3. Optical and EPR spectroscopy were employed to examine pH-dependent changes for the phosphate complexes of both Fe(III)Fe(II)−BSPAP and Fe(III)Zn(II)−BSPAP. To determine whether the phosphate complexes were good structural models for the enzyme−substrate complexes, the latter complexes were studied directly using rapid-freeze EPR and stopped-flow optical spectroscopy. We propose that both phosphate and *p*-NPP bridge the two metal ions at low pH. At higher pH, where the enzyme is optimally active, our results suggest that hydroxide competes with phosphate and *p*-NPP for coordination to Fe^{3+} and that both phosphate and *p*-NPP coordinate only to the divalent metal ion.

EXPERIMENTAL PROCEDURES

General. Bovine spleen purple acid phosphatase was isolated as previously described (*22*). Preparations had $A_{280\ nm}/A_{536\ nm}$ ratios of 14−15. FeZn−BSPAP was prepared as described previously (*4*). Protein concentrations were determined by measuring the absorption of the tyrosinate-to-Fe^{3+} charge-transfer band at ∼530 nm (ϵ = 4080 $M^{-1}\cdot cm^{-1}$). The various equations were fitted using the nonlinear least-squares fit procedure in the program IGOR (WaveMetrics).

Enzyme Kinetics. Enzyme assays were performed by monitoring the formation of *p*-nitrophenolate at 410 nm. At several times after enzyme addition, 500 μL aliquots were taken and quenched by mixing with 1.5 mL 0.5 M NaOH to convert all product to the phenolate form ($\epsilon_{410\ nm}$ = 16.6 $mM^{-1}\cdot cm^{-1}$). Since BSPAP is partly inactivated in dilute solutions (*23*), enzyme stock solutions contained 0.5 mg/mL BSA to prevent inactivation. The pH dependence of Fe(III)Fe(II)−BSPAP was measured in 100 mM buffer (NaOAc, Na−MES, or Na−HEPES), 185 mM KCl, 15 mM Na−ascorbate, 0.2 mM $Fe(NH_4)_2(SO_4)_2$, and various concentrations of *p*-NPP. The pH dependence of Fe(III)Zn(II)−BSPAP was measured in 100 mM buffer (NaOAc, Na−MES, or Na−HEPES), 200 mM KCl, and various concentrations of *p*-NPP. The pH values were measured immediately at the end of the assay (2 min after the addition of enzyme). For each determination of K_M and V_{max}, the hydrolysis rate was measured at 10 different *p*-NPP concentrations between 0.3 mM and 50 mM. Values of K_M and V_{max} were obtained by a nonlinear fit of the Michaelis−Menten equation using the program EnzymeKinetics (Trinity Software). K_i values for

phosphate were determined using the same program, by measuring hydrolysis rates at different *p*-NPP concentrations and several fixed phosphate concentrations.

EPR Spectroscopy. X-band EPR spectra (9.4 GHz) were obtained on a Bruker ECS106 EPR spectrometer, equipped with an Oxford Instruments ESR900 helium-flow cryostat with an ITC4 temperature controller. The magnetic field was calibrated with an AEG Magnetic Field Meter. The frequency was measured with an HP 5350B Microwave Frequency Counter.

Phosphate titrations of FeZn−BSPAP were performed by repeated addition of small aliquots of concentrated KH_2PO_4/K_2HPO_4 stock solutions of the appropriate pH to a single sample of FeZn−BSPAP in 100 mM buffer (NaOAc/pH 5 or Na−MES/pH 6.5) and 200 mM KCl. Samples of Fe(III)-Fe(II)−BSPAP·PO_4 were prepared under anaerobic conditions to prevent oxidation to the stable Fe(III)Fe(III)−BSPAP·PO_4 form. For the phosphate titrations at pH 5 and 6.5, a series of EPR tubes was filled with Fe(III)Fe(II)−BSPAP in 100 mM buffer (NaOAc/pH 5.0 or Na−MES/pH 6.5) and 200 mM KCl. The samples were made anaerobic by repeated vacuum/argon cycles. Different amounts of anaerobic KH_2PO_4/K_2HPO_4 stock solutions of the appropriate pH were added, mixed, and the samples were frozen immediately in liquid nitrogen. For the pH titration of Fe-(III)Fe(II)−BSPAP·PO_4, EPR tubes were filled with ∼150 μM solutions of Fe(III)Fe(II)−BSPAP in 100 mM buffer (NaOAc/pH 4.5−5.5, Na−MES/pH 5.5−6.5, and Na−MOPS/pH 7.0) and 200 mM KCl. EPR spectra of the uncomplexed BSPAP were measured and spin concentrations were determined by double integration of these spectra and the spectrum of a Cu^{2+} standard. Appropriate corrections were made for differences in *g* values between the standard and the sample (*40*, *41*). The samples were thawed, made anaerobic, phosphate was added anaerobically, and the samples were frozen again. The signal intensities of the EPR spectra of the phosphate complexes were corrected for differences in spin concentrations of the samples before addition of phosphate.[2] The determination of K_d values was performed as previously described (*4*).

Optical Spectroscopy. Optical spectra were measured on a Cary 50 spectrophotometer (Varian). The pH dependence of the optical spectra of Fe(III)Zn(II)−BSPAP was measured by addition of ∼5 μL of a nonbuffered, concentrated protein solution to 95 μL buffer solution containing 90 mM buffer (Na−MOPS, Na−MES, or NaOAc), 180 mM KCl and 100 mM phosphate. The spectra were normalized to give the same absorbance of the tyrosinate-to-Fe^{3+} charge-transfer band at 530−560 nm. The optical spectra of Fe(III)Fe(II)−BSPAP·PO_4 complexes were measured in septum-stoppered cuvettes under semi-anaerobic conditions to prevent oxidation to the Fe(III)Fe(III)·PO_4 complexes. Cuvettes with 500 μL buffer containing 90 mM buffer (Na−MOPS, Na−MES, or NaOAc), 180 mM KCl, and 100 mM phosphate were made anaerobic by repeated vacuum/argon cycles. Under a flow of argon 15 μL of a nonbuffered, concentrated protein solution was added, and a spectrum was obtained immediately. No significant oxidation was observed under these conditions during the time scale of the experiment. The spectra were normalized to give the same absorbance of the tyrosinate-to-Fe^{3+} charge-transfer band at 500−560 nm.

Stopped-Flow Optical Spectroscopy. Stopped-flow experiments were carried out on an Union-Giken RA-401 spectrophotometer. A 2 mm path length cuvette was used, resulting in a dead time of 0.7 ms. The formation of *p*-nitrophenol was monitored at 400 nm ($\epsilon_{pH\ 7.0}$ = 7800 $M^{-1}\cdot cm^{-1}$). Measurements were performed at 7 °C to decrease the value of k_{cat} to ∼400 s^{-1}, in order to increase the possibility of detecting a burst of *p*-nitrophenol upon mixing enzyme and substrate. Reservoir 1 contained 46.6 μM Fe(III)Fe(II)−BSPAP, 50 mM MOPS, 50 mM KCl, 30 mM Na−ascorbate, and 0.3 mM $Fe(NH_4)_2(SO_4)_2$, pH 7.0. Reservoir 2 contained 40 mM *p*-NPP, 50 mM MOPS, and 50 mM KCl, pH 7.0. To determine the background absorption, control experiments in which substrate was mixed with the same buffer without the enzyme were done immediately before and after the experiment. Each experiment consisted of 4−5 shots, and the resulting traces were averaged to obtain better signal-to-noise levels.

Rapid-Freeze EPR Spectroscopy. Rapid-mixing rapid-freezing experiments were performed at ambient temperatures (23 ± 1 °C) using a home-built freeze-quench apparatus (*42*). The dead-time of this apparatus is about 5 ms. For pH 5.0, 0.73 mM Fe(III)Fe(II)−BSPAP in 100 mM NaOAc, 200 mM KCl pH 5.0 was mixed with 100 mM *p*-NPP or 100 mM KH_2PO_4/K_2HPO_4 in 100 mM NaOAc, 200 mM KCl pH 5.0. For pH 6.5, 0.45 mM $Fe^{3+}Fe^{2+}$−BSPAP in 100 mM Na−MES, 200 mM KCl pH 6.5 was mixed with 100 mM *p*-NPP or 100 mM KH_2PO_4/K_2HPO_4 in 100 mM Na−MES, 200 mM KCl pH 6.5. The reaction was quenched by spraying the sample into cold isopentane at a temperature of ∼140 K.

RESULTS

pH Dependence of Kinetics Parameters. To provide a firm basis for the interpretation of pH dependent changes in spectroscopic properties, the kinetics parameters k_{cat} and K_M were determined for the hydrolysis of *p*-NPP over the pH range 3.5 to 8.5. Because previous studies at fixed concentrations of *p*-NPP showed small but significant differences between the pH dependence of the Fe(III)Fe(II) and Fe(III)-Zn(II) enzymes, both BSPAP forms were studied (*4*). Since the activity of BSPAP is somewhat ionic strength dependent, all buffers contained 200 mM KCl and 100 mM of the sodium salt of the buffer (NaOAc, Na−MES, or Na−HEPES). No specific buffer effects were observed. Figure 1 shows the pH dependence of k_{cat}, k_{cat}/K_M, and K_M for both Fe(III)Fe(II)−BSPAP and Fe(III)Zn(II)−BSPAP. Since the k_{cat} vs pH plot shows a symmetric bell-shaped curve, the pH dependencies were analyzed according to the rapid equilibrium diprotic model shown in Scheme 1 (*43*). If it is assumed that all equilibria in Scheme 1 are rapidly established compared to k_{cat}, the following expressions can be derived for the observed values for k_{cat}, k_{cat}/K_M, and K_M at a given pH:

$$k_{cat(observed)} = k_{cat}/(1 + [H^+]/K_{es1} + K_{es2}/[H^+]) \quad (1)$$

[2] The samples at pH >5.5 showed consistently lower spin concentrations, presumably because of oxidation taking place during buffer exchange.

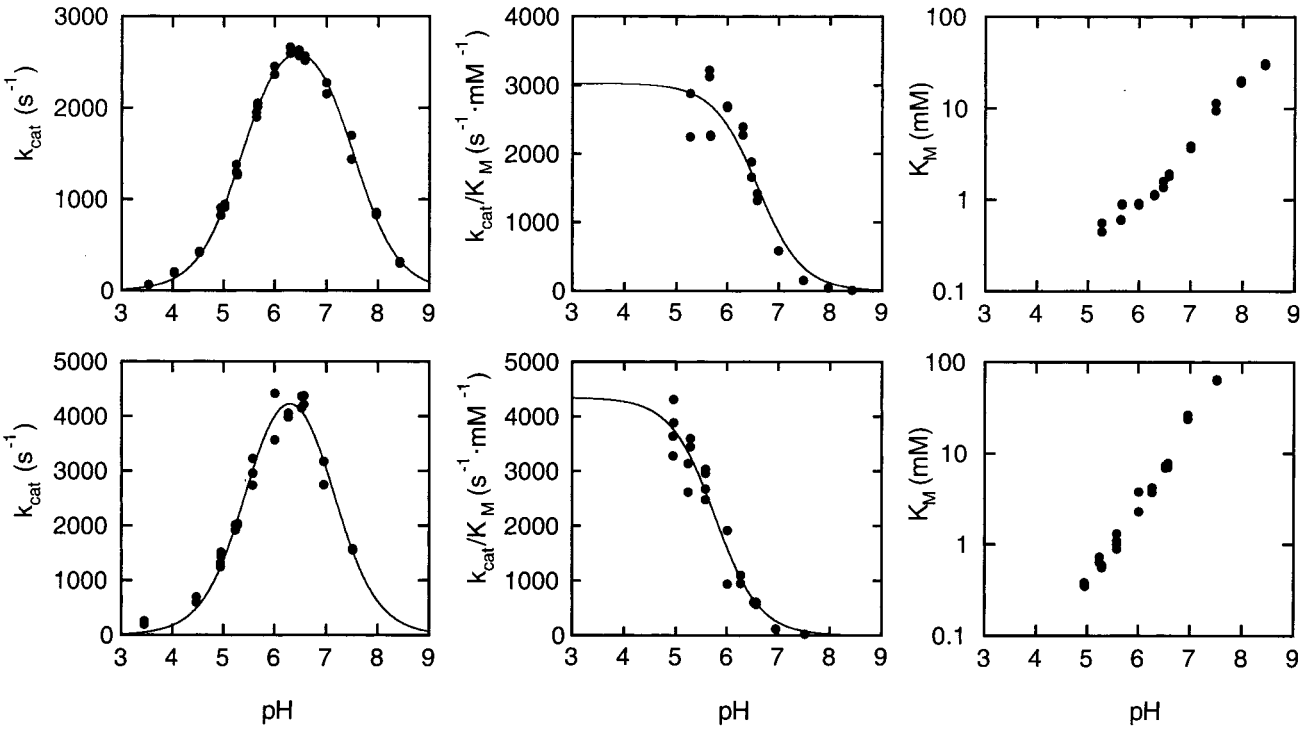

FIGURE 1: pH dependencies of $k_{cat(apparent)}$, $k_{cat(apparent)}/K_{M(apparent)}$, and $K_{M(apparent)}$ for Fe(III)Fe(II)−BSPAP (upper panels) and Fe(III)Zn(II)−BSPAP (lower panels) with *p*-NPP as substrate at 22 °C. The lines in the $k_{cat(apparent)}$ and $k_{cat(apparent)}/K_{M(apparent}$ profiles represent best fits to eq 1 and 2, respectively. Fe(III)Fe(II)−BSPAP: 100 mM buffer (NaOAc, Na−MES, or Na−HEPES), 185 mM KCl, 15 mM Na−ascorbate, and 0.2 mM $Fe(NH_4)_2(SO_4)_2$. Fe(III)Zn(II)−BSPAP: 100 mM buffer (NaOAc, Na−MES, or Na−HEPES) and 200 mM KCl.

$$k_{cat(observed)}/K_{M(observed)} = k_{cat}/K_S(1 + [H^+]/K_{e1} + K_{e2}/[H^+]) \quad (2)$$

$$K_{M(observed)} = K_S(1 + [H^+]/K_{e1} + K_{e2}/[H^+])/(1 + [H^+]/K_{es1} + K_{es2}/[H^+]) \quad (3)$$

The pK_a values derived from the k_{cat} vs pH profile correspond to protonation equilibria in the enzyme−substrate complex, while the k_{cat}/K_M vs pH profile is determined by protonation equilibria of the free enzyme or the free substrate. Table 1 contains the kinetics constants as they were determined from fitting the $k_{cat(observed)}$ and $k_{cat(observed)}/K_{M(observed)}$ profiles to eqs 1 and 2, respectively. For Fe(III)Zn(II)−BSPAP, K_M values became too high at pH >7.5 to obtain reliable kinetics parameters. At low pH, the K_M became too low to allow the reliable determination of K_M values for both BSPAP forms. The k_{cat}/K_M profile could be fitted using a single pK_a (pK_{e2}) (assuming pK_{e1} < 2), but the lack of reliable data at pH <5.5 means that some care should be exercised in interpreting these data.

pH Dependence of Spectral Properties of Phosphate Complexes. The pH dependence of k_{cat} shown in Figure 1 suggests that at pH 5.0 the enzyme−substrate complex is primarily in a catalytically inactive form. Since most previous spectroscopic studies on PAP were carried out at pH 5.0, we decided to (re)investigate the optical and EPR properties of the phosphate complex, both at pH 5 and at higher pH values, where the catalytically active protonation state of the enzyme−substrate complex exists. The availability of both the (native) Fe(III)Fe(II) and Fe(III)Zn(II) forms of BSPAP allowed us to distinguish between perturbations that affect the Fe(III) from perturbations that affect only the divalent metal ion.

Table 1: Kinetics Constants as Determined from the pH Dependence of Phosphatase Activity for Fe(III)Fe(II)− and Fe(III)Zn(II)−BSPAP

enzyme	pK_{es1}[a]	pK_{es2}[a]	k_{cat} (s^{-1})[a]	K_S (mM)[b]	pK_{e2}[b]
Fe(III)Fe(II)−BSPAP	5.4	7.5	3.0×10^3	1.0	6.6
Fe(III)Zn(II)−BSPAP	5.5	7.1	5.5×10^3	1.3	5.7

[a] Obtained from a fit of k_{cat} as a function of pH using eq 1. [b] Obtained from a fit of k_{cat}/K_M as a function of pH using eq 2, with pK_{e1} < 2.

Scheme 1

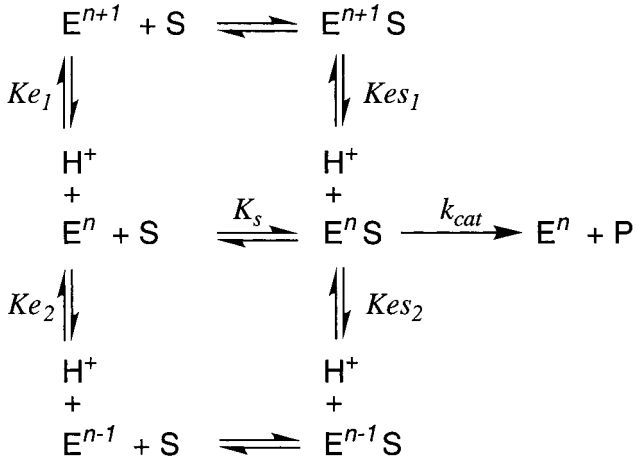

Figures 2 and 3 show that at pH 5.0 the EPR spectra of both Fe(III)Fe(II)−BSPAP and Fe(III)Zn(II)−BSPAP are affected by the addition of phosphate. The native Fe(III)-Fe(II)−BSPAP spectrum is converted to a broad spectrum that consists of at least two species (Figure 2). The feature at $g \sim 2.25$ is probably due to the same species that gives rise to the broad, anisotropic rhombic spectrum reported for

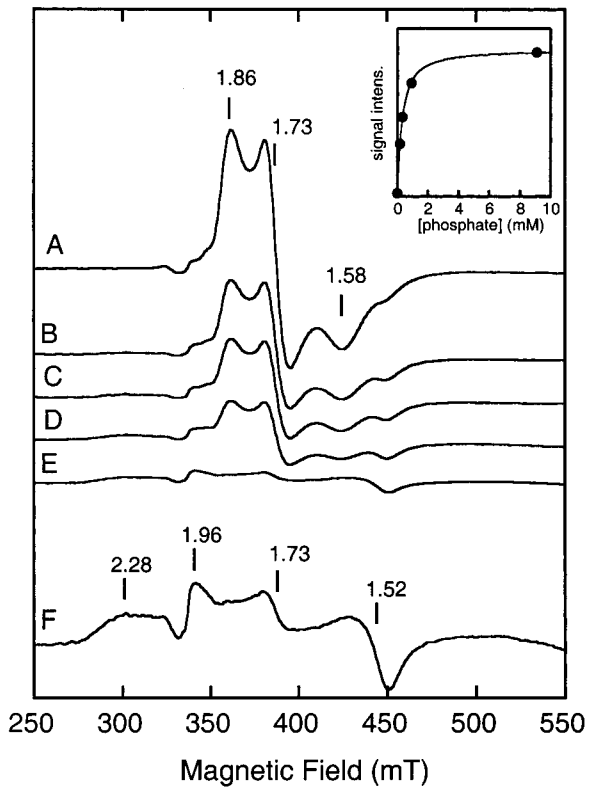

FIGURE 2: EPR titration showing the conversion from Fe(III)Fe(II)−BSPAP to Fe(III)Fe(II)−BSPAP·PO_4 at pH 5.0. Spectra were collected at (A) 0, (B) 0.18, (C) 0.33, (D) 0.91, and (E, F) 9.1 mM phosphate and ∼0.15 mM protein in 90 mM NaOAc, 180 mM KCl, pH 5.0. Spectrum F is spectrum E after 5-fold enlargement. EPR conditions: microwave power, 20 mW; microwave frequency, 9.42 GHz; modulation, 28.5 G at 100 kHz; temperature, 4.5 K. Inset: difference of the normalized intensities at $g = 2.28$ and 1.86 as a function of phosphate concentration. The solid line describes a fit with $K_d = 0.24$ mM.

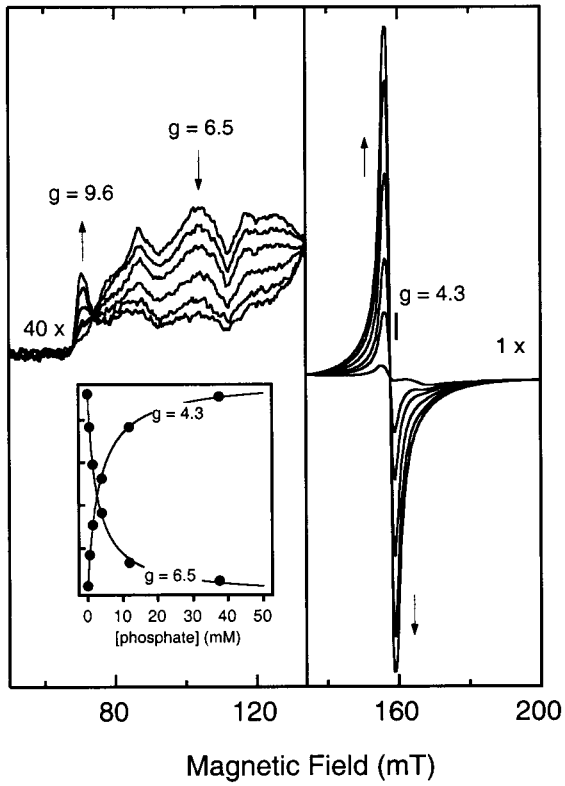

FIGURE 3: EPR titration showing the conversion from Fe(III)Zn(II)−BSPAP to Fe(III)Zn(II)−BSPAP·PO_4 at pH 5.0. Spectra were collected at 0, 0.56, 1.4, 4.0, 12, and 38 mM phosphate and 80 μM protein in 100 mM NaOAc, 200 mM KCl, pH 5.0. The arrows indicate increasing phosphate concentration. EPR conditions: microwave power, 2.0 mW; microwave frequency, 9.415 GHz; modulation, 12.7 G at 100 kHz; temperature, 10.0 K. Inset: intensity at $g = 4.3$ and 6.5 as a function of phosphate concentration. The solid lines describe binding curves for K_d values of 3.5 and 2.6 mM, respectively.

Fe(III)Fe(II)−Uf·PO_4, which showed *g*-values at 2.25, 1.5, and ∼1.1 (*8*). The feature at $g = 1.52$ seems to also be present in the EPR spectrum of the uncomplexed Fe(III)Fe(II)−BSPAP, and may be due to a small amount of the protein that is not able to bind phosphate. The signals at $g = 1.94$ and 1.73 were also reported for Fe(III)Fe(II)−Uf·PO_4, but were ascribed to uncomplexed protein. No large difference in the intensities of these signals is seen, however, between the spectra obtained in the presence of 9.1 mM and 55 mM PO_4, indicating that these features are probably not due to uncomplexed enzyme. The conversion of the broad EPR spectrum of free Fe(III)Zn(II)−BSPAP to the sharp isotropic $g = 4.3$ signal of the phosphate complex has been reported previously, both for BSPAP (*4*, *20*) and for Uf (*10*). Fits of signal intensities as a function of phosphate concentration gave K_d values of 0.24 mM for Fe(III)Fe(II)−BSPAP and ∼3 mM for Fe(III)Zn(II)−BSPAP.

Since the EPR spectrum of Fe(III)Fe(II)−BSPAP·PO_4 showed the presence of at least two different species, the possibility was considered that these species were due to differently protonated forms of the phosphate complex. EPR spectra were measured for Fe(III)Fe(II)−BSPAP·PO_4 at several pH values from pH 4.5 to 7.0. Figure 4 shows that at higher pH a new phosphate complex is formed, with apparent *g*-values of 1.94, 1.71, and 1.50. The EPR signal of this high-pH form is more intense than that of the low-pH form and is more similar to that of the free enzyme. Loss of signal intensity starts to occur at T > 8K for this species, probably due to population of higher spin states. Relaxation is fast even at 5.0 K, with $P_{1/2} \approx 100$ mW. The relative peak intensities at $g = 2.25$ were subtracted from the relative peak intensities at $g = 1.94$, and the resulting signal intensities were plotted as a function of pH (inset Figure 4). The curve describes the best fit of these data using the Henderson−Hasselbalch equation ($n = 1$) and a pK_a of 6.

The pH titration shown in Figure 4 shows the presence of a new phosphate complex at pH 6.5−7.0, which corresponds to the pH at which the amount of the active form of the enzyme−substrate complex is maximal. Phosphate titrations were, therefore, also done at pH 6.5 for both Fe(III)Fe(II)−BSPAP (Figure 5) and Fe(III)Zn(II)−BSPAP (Figure 6). Figure 5 shows the EPR spectra of Fe(III)Fe(II)−BSPAP at different phosphate concentrations. A fit of the difference between the signal intensities at $g = 1.86$ and 1.94 as a function of phosphate concentration gave a K_d value of 0.7 mM. In contrast to Fe(III)Fe(II)−BSPAP, the EPR spectrum of Fe(III)Zn(II)−BSPAP is not affected significantly by phosphate concentrations of ≤30 mM (Figure 6). It should be noted that the Fe(III)Zn(II)−BSPAP EPR spectrum is converted to a sharp isotropic $g = 4.3$ signal in the presence of very high phosphate concentrations at pH 6.5. A plot of

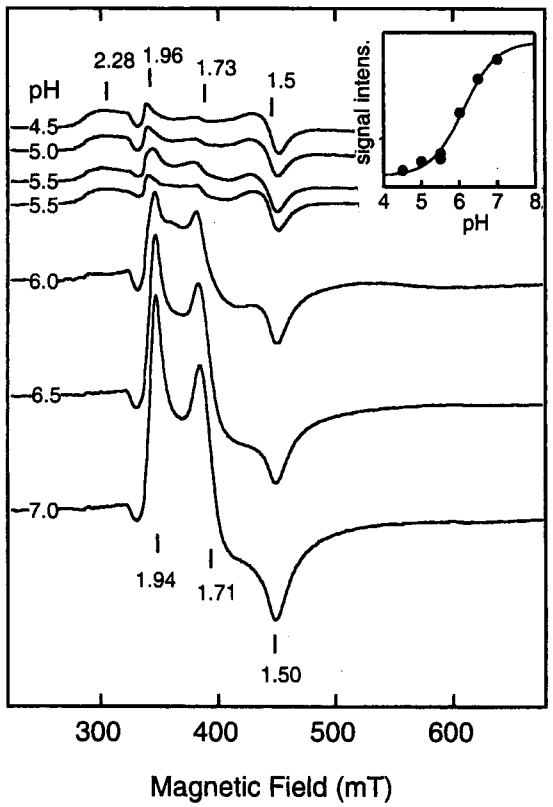

FIGURE 4: EPR spectra of Fe(III)Fe(II)−BSPAP·PO_4 as a function of pH. Samples contained ∼0.12 mM protein in 90 mM buffer (NaOAc, Na−MES, or Na−MOPS), 180 mM KCl and 56 mM phosphate. Spectral amplitudes were corrected for differences in spin concentrations as determined before addition of phosphate. EPR conditions: microwave power, 20 mW; microwave frequency, 9.41 GHz; modulation, 28.5 G at 100 kHz; temperature, 4.5 K. Inset: difference of the normalized intensities at $g = 2.25$ and 1.94 as a function of pH. The solid line describes the best fit of these data using the Henderson−Hasselbalch equation ($n = 1$) and a pK_a of 6.

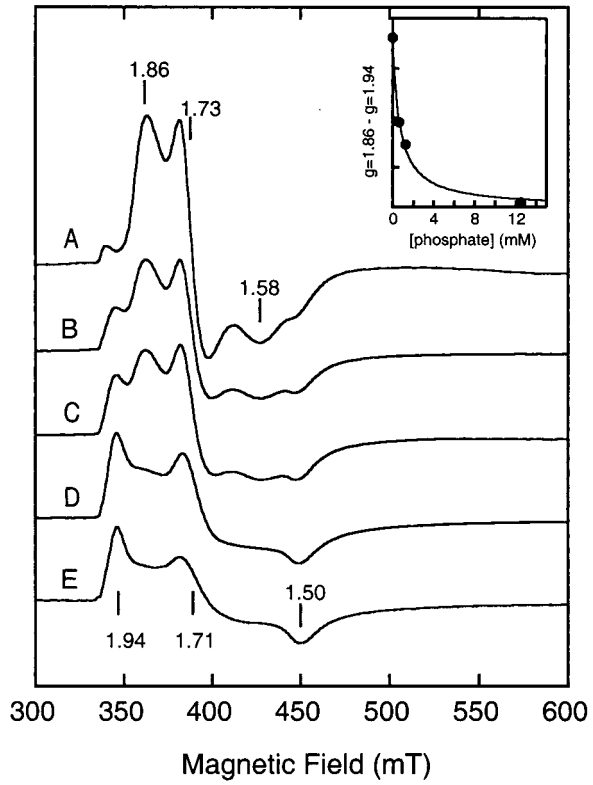

FIGURE 5: EPR titration showing the conversion from Fe(III)Fe(II)−BSPAP to Fe(III)Fe(II)−BSPAP·PO_4 at pH 6.5. Spectra were collected at (A) 0, (B) 0.63, (C) 1.25, (D) 12.5, and (E) 125 mM phosphate and ∼90 μM protein in 90 mM Na−MES, 180 mM KCl, pH 6.5. EPR conditions: microwave power, 20 mW; microwave frequency, 9.41 GHz; modulation, 28.5 G at 100 kHz; temperature, 4.5 K. Inset: The difference of the intensities of the $g = 1.86$ and 1.94 signals as a function of phosphate concentration. The solid line describes a fit with $K_d = 0.7$ mM.

the signal intensity at $g = 4.3$ as a function of phosphate concentration remains linear even up to 300 mM phosphate (Figure S1 of the Supporting Information), however, indicating that this effect of phosphate may be due to changes in the ionic strength, possibly affecting pK_a values of active site groups. An inhibition constant for phosphate of 2 mM was determined for Fe(III)Zn(II)−BSPAP at pH 6.5. Thus, it may be concluded that, in contrast to Fe(III)Fe(II)−BSPAP, binding of the inhibitor phosphate does not result in significant changes in the EPR spectrum of Fe(III)Zn(II)−BSPAP.

To establish that the pH-dependent effects described above for k_{cat} and the EPR spectrum of the phosphate complex are also linked to changes in the optical spectra of the phosphate complex, optical spectra were obtained for Fe(III)Fe(II)−BSPAP·PO_4 and Fe(III)Zn(II)−BSPAP·PO_4 in the pH range 4.0 to 7.5. Figure 7 shows that λ_{max} of Fe(III)Fe(II)−BSPAP·PO_4 shifts from 561 nm at pH 4.0 to 500 nm at pH 7.5, while λ_{max} of Fe(III)Zn(II)−BSPAP·PO_4 shifts from 563 nm at pH 4.0 to 537 nm at pH 7.5. The insets show plots of λ_{max} as a function of pH. For both species, the curves describe fits of the Henderson−Hasselbalch equation with $n = 1$ and pK_a's of 5.4 ± 0.1.

Burst Kinetics. The turnover rate for the hydrolysis of *p*-NPP by BSPAP of ∼2000 s^{-1} (22 °C; pH 6.00) makes it difficult to use pre-steady-state kinetics methods to study transient intermediates in BSPAP catalysis. The application of rapid-mixing rapid-detection techniques can, however, still be useful, since they allow the characterization of the enzyme intermediate that precedes the rate-limiting step in catalysis. A minimal catalytic mechanism for PAP is depicted in Scheme 2. The first step is the formation of an enzyme−substrate complex. In the second step, the substrate is hydrolyzed and *p*-nitrophenol (*p*NP) is released. In the final step, the second product, phosphate, is released. It is reasonable to assume that the alcohol is released first, because *p*NP does not inhibit the enzyme, while phosphate does (*44*). If $k_3 < k_2$, so that release of phosphate is rate-limiting, mixing enzyme with substrate will result in rapid formation of one equivalent of *p*NP ("burst"), followed by a slower formation of *p*NP at a rate equal to k_3 (*45*). If $k_2 < k_3$, then no burst of *p*NP will be observed and the rate of *p*NP release will be linear immediately after mixing and equal to k_2. We used stopped-flow optical spectroscopy to determine whether BSPAP exhibited burst kinetics at pH 7.0: at this pH the enzyme still shows ∼85% of maximal activity. The product *p*NP also has a reasonably large extinction coefficient (7800 M^{-1}·cm^{-1}) at pH 7.0, which is necessary to be able to detect the burst (at pH 6.3, the extinction coefficient is only 2300 M^{-1}·cm^{-1}). The upper trace in Figure 8 was obtained when Fe(III)Fe(II)−BSPAP was mixed with 40 mM *p*-NPP at pH 7.0 and 7 °C. During the first 22 ms, the mixed solution

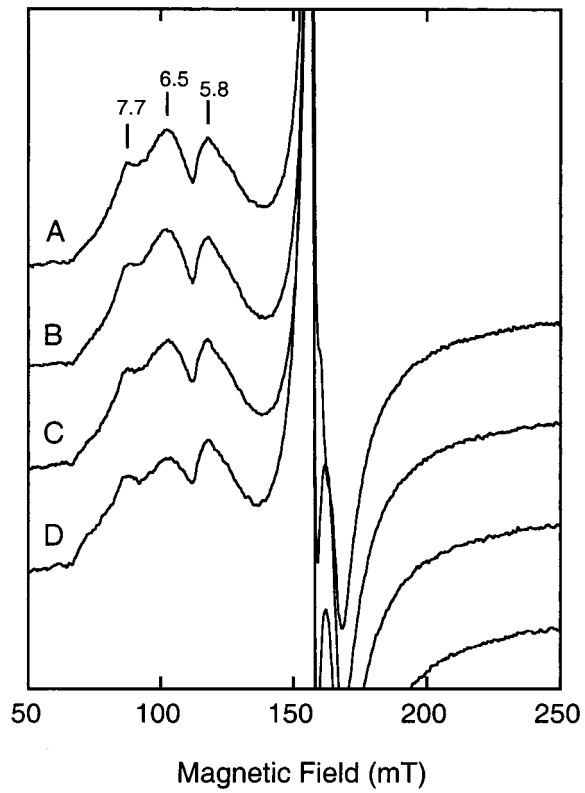

FIGURE 6: EPR spectra of Fe(III)Zn(II)−BSPAP in the presence of various phosphate concentrations at pH 6.5. Spectra were collected at (A) 0, (B) 2.0, (C) 7.9, and (D) 31 mM phosphate and 80 μM protein in 100 mM NaOAc, 200 mM KCl, pH 6.5. EPR conditions: microwave power, 2.0 mW; microwave frequency, 9.415 GHz; modulation, 12.7 G at 100 kHz; temperature, 10.0 K.

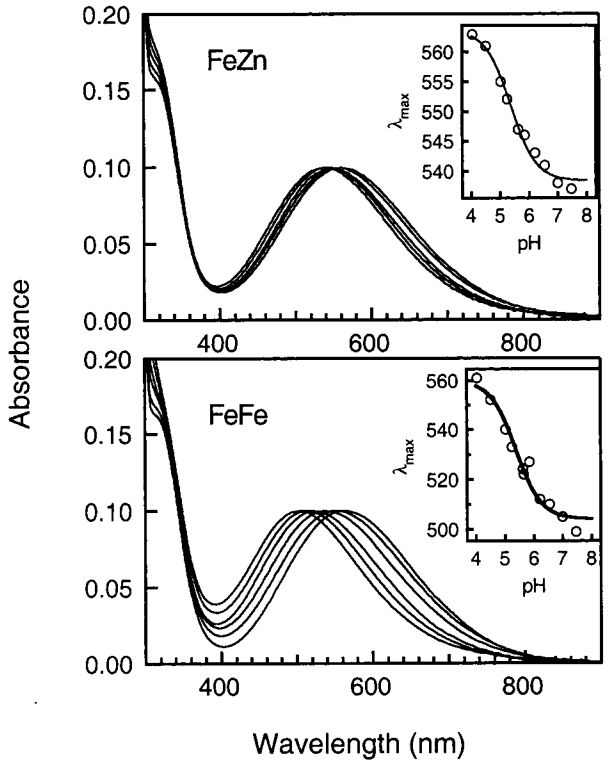

FIGURE 7: Optical spectra of Fe(III)Zn(II)−BSPAP·PO_4 (upper panel) and Fe(III)Fe(II)−BSPAP·PO_4 (lower panel) as a function of pH in the range pH 4.0 to 7.5. Conditions: 90 mM buffer (Na−MOPS, Na−MES, NaOAc), 180 mM KCl, 100 mM phosphate. Insets: λ_{max} as a function of pH. The lines describe fits of the Henderson−Hasselbalch equation with pK_a = 5.4 (n=1).

was still flowing through the cuvette. The absorbance in this part of the figure reflects the absorbance of the mixed solution after the dead time of the instrument, i.e., 0.7 ms. At 22 ms, the flow was stopped and the reaction was allowed to develop. The lower traces are control experiments in which substrate was mixed with buffer without enzyme. The expected absorbance levels (at t = 0.7 ms) in the case of burst kinetics and in the case of the absence of burst kinetics are also depicted in Figure 8.[3] Thus, it can be concluded that BSPAP does not show burst kinetics at pH 7.0. Figure 8 also shows that BSPAP is active immediately and does not require substrate-induced activation. The absence of burst kinetics is consistent with either the binding of substrate or the hydrolysis of the substrate as the rate-limiting step.[4]

Trapping and EPR Characterization of Fe(III)Fe(II)−BSPAP-p-NPP Complexes. The pH dependence of the spectroscopic properties of the phosphate complexes and the pH dependence of k_{cat} for the hydrolysis of *p*-NPP both show the presence of an acid−base equilibrium with a pK_a of ∼5.5. This implies that the same protonation event is responsible for the inactivation of the enzyme−substrate complex at low pH and the conversion of the high-pH to low-pH phosphate complex. Since the stopped-flow measurements indicated that hydrolysis of the substrate is probably rate-limiting (rate-limiting substrate binding is less likely, vide infra), it should in principle be possible to trap the enzyme−substrate complex by mixing enzyme and saturating amounts of substrate rapidly, followed by rapid freezing of the mixture in cold isopentane. Because of the high turnover rates (∼800 s^{-1} at pH 5.0 and ∼2400 s^{-1} at pH 6.5 and 22 °C), steady-state conditions are reached within 1−2 ms. Because of the relatively high-protein concentrations needed for EPR detection of the phosphate complexes, reaction times that are substantially longer than 5 ms would result in the hydrolysis of most of the substrate before the mixture could be frozen.[5]

Scheme 2

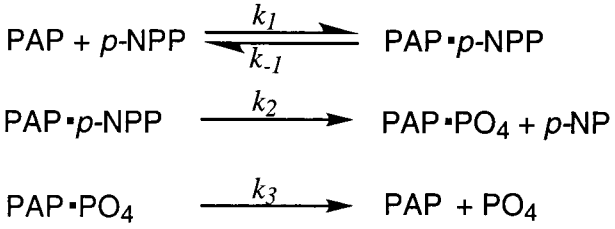

[3] In the absence of burst kinetics, the absorbance level for the enzyme−substrate mixture will still be 0.0144 au higher than the control experiments due to the absorbance of the protein (23.3 μM × 1200 M^{-1}·cm^{-1} × 0.2 cm = 0.0056 au) and the product formed in the dead-time of the reaction (0.7 ms × 12.5 au/s = 0.0088 au). Equation 4 ($1/\sqrt{\pi} = (1/\sqrt{[E]_0})(1 + k_3/k_2 + (K_M k_2)/([S]k_{cat}))$ can be used to calculate the amount of *p*NP (π) formed during the burst. If $k_3 \ll k_2$, then the burst will be equal to 1.0 × $[E]_o$ = 23.3 μM, corresponding to an absorbance of 0.0363. In the presence of burst kinetics, the absorbance level will, therefore, be 0.0144 + 0.0363 = 0.0507 au higher than the absorbance level of the control experiment.

[4] If $k_2 = k_3$, then eq 4 predicts the formation of a substoichiometric burst of ∼0.25 equivalents of *p*-NP when [S] ≫ K_M. Since such a small burst would be difficult to detect, we cannot rule out this possibility on the basis of our stopped-flow optical experiment alone.

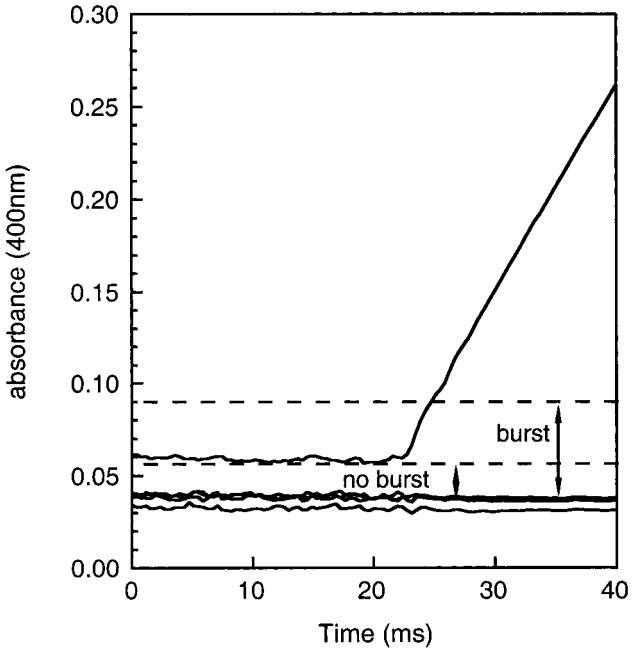

FIGURE 8: Stopped-flow trace of the absorbance at 400 nm after mixing of 46.6 μM Fe(III)Fe(II)−BSPAP in 50 mM MOPS, 50 mM KCl, 30 mM Na−ascorbate, and 0.3 mM Fe(NH4)2(SO4)2, pH 7.0 (syringe 1) with 40 mM *p*-NPP in 50 mM MOPS, 50 mM Kcl, pH 7.0 (syringe 2) at 7 °C. The lower traces are control reactions where the substrate solution was mixed with buffer without protein. The first ~20 ms represent the absorbance of the mixture when it is still flowing through the cell. The upper dashed line represents the absorbance level expected for the case of burst kinetics. The lower dashed line represents the absorbance level in the absence of burst kinetics.

Fe(III)Fe(II)−BSPAP was mixed with 100 mM *p*-NPP and freeze-quenched in cold isopentane as quickly as possible (~5 ms), both at pH 5.0 and pH 6.5. For comparison, the same protein batches were also mixed with 100 mM phosphate at the appropriate pH and freeze-quenched.

Figure 9 shows the EPR spectra of the Fe(III)Fe(II)−BSPAP·*p*-NPP and Fe(III)Fe(II)−BSPAP·PO_4 complexes obtained by freeze-quenching at pH 5.0 and pH 6.5. The EPR spectra of Fe(III)Fe(II)−BSPAP·*p*-NPP and Fe(III)Fe(II)−BSPAP·PO_4 are very similar, both at pH 5.0 and pH 6.5. The spectrum of the *p*-NPP complex at pH 5.0 looks very similar to that of the phosphate complex obtained by slow freezing in liquid nitrogen (Figure 2). The contribution of the features at $g = 1.94$ and 1.73 is somewhat larger in the spectrum of the pH 5.0 freeze-quenched phosphate sample, possibly indicating that the binding of phosphate in the latter is not yet complete after 5 ms. At pH 6.5, very similar spectra are also obtained for the phosphate and *p*-NPP complexes. The phosphate spectrum shown in Figure 9 shows a single rhombic species, but some of the samples (both of the phosphate and of the *p*-NPP complexes) also contained a small amount of the uncomplexed enzyme. Careful inspection of the pH 6.5 spectra reveals small but significant differences between the EPR spectra of the *p*-NPP and phosphate complex. The difference is most clearly seen in g_x, which is at 1.955 for Fe(III)Fe(II)−BSPAP-*p*-NPP and

[5] For the pH 6.5 samples, 0.005 s × 2400 s^{-1} × 225 μM = 2.7 mM of *p*-NPP is hydrolyzed within 5 ms. At pH 5.0, 0.005 s × 800 s^{-1} × 365 μM = 1.46 mM of *p*-NPP is hydrolyzed within 5 ms.

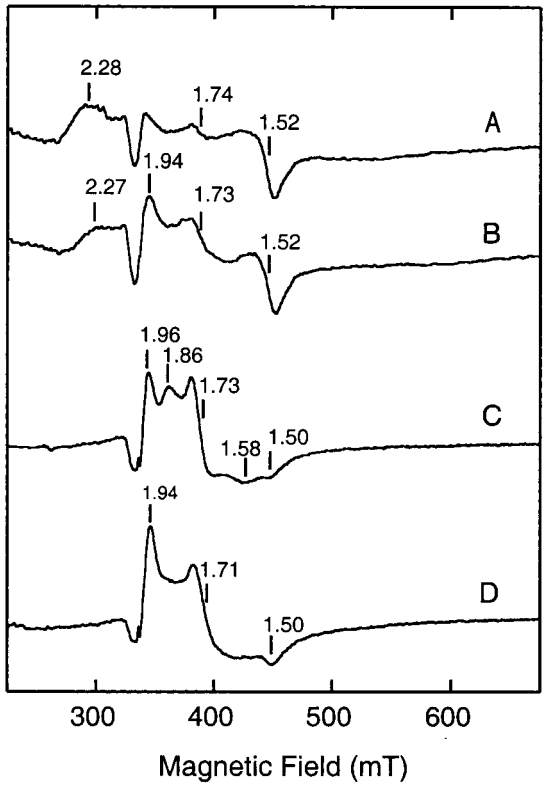

FIGURE 9: EPR spectra of reaction mixtures that were freeze-quenched 5 ms after mixing (A) 0. 37 mM Fe(III)Fe(II)−BSPAP with 50 mM *p*-NPP at pH 5.0, (B) 0. 37 mM Fe(III)Fe(II)−BSPAP with 50 mM phosphate at pH 5.0, (C) 0.23 mM Fe(III)Fe(II)−BSPAP with 50 mM *p*-NPP at pH 6.5, and (D) 0.23 mM Fe(III)-Fe(II)−BSPAP with 50 mM phosphate at pH 6.5. Buffer: 100 mM NaOAc (pH 5.0) or NaMES (pH 6.5), and 200 mM KCl. EPR conditions: microwave power, 20 mW; microwave frequency, 9.43 GHz; modulation, 12.7 G at 100 kHz; temperature, 4.5 K. After corrections for differences in protein concentration and gain, the spectral amplitudes of the pH 5.0 spectra were 3-fold enlarged relative to the spectra at pH 6.5.

at 1.944 for Fe(III)Fe(II)−BSPAP·PO_4 (both in the freeze-quenched samples and in the samples obtained by slow freezing in liquid nitrogen). The position of g_y is also different (~1.73 for *p*-NPP and ~1.71 for PO_4), but the apparent position of g_y is also sensitive to the presence of small amounts of uncomplexed protein, making this point less certain. The fact that the EPR spectrum of the complex with *p*-NPP at pH 6.5 is similar but not identical to that of the phosphate complex indicates that, under steady-state conditions, most of the enzyme is present as the enzyme−substrate complex rather than the enzyme−phosphate complex or the uncomplexed form; this is consistent with the finding from the stopped-flow optical experiment that hydrolysis of *p*-NPP is rate-limiting.

DISCUSSION

pH Dependence of Kinetics Parameters. Before one can meaningfully interpret the results of structural studies on an enzyme and its complexes with substrate analogues, it is essential to know under which conditions (pH, substrate concentration) the enzyme is optimally active. The pH dependence studies reported herein show that at pH 5.0 (the pH used in most previous spectroscopic and structural studies on PAPs), most of the enzyme is in a catalytically inactive

protonation state. The pK_a of 5.4−5.5 that is found for the acidic limb of the k_{cat} vs pH profile of both the Fe(III)Fe(II) and the Fe(III)Zn(II) form may be due to an Fe^{3+}-coordinated water in the enzyme−substrate complex. The hydroxide formed at pH > 5.5 may be the hydroxide that is proposed to attack the phosphate ester (*11*, *18*, *36*). Consistent with this assignment is the fact that this pK_a is unaffected by substitution of the divalent metal ion, but shifts to somewhat lower values when Fe^{3+} is replaced by Ga^{3+} (although for Al^{3+} it is similar) (*22*, *37*). This interpretation is also supported by the pH dependence of the spectral properties of the phosphate complex, which may be considered as a model for the enzyme−substrate complex (vide infra). pK_{es2} is due to a group in the enzyme−substrate complex that needs to be protonated for catalysis to take place, possibly the group responsible for protonation of the phenoxide leaving group. The sensitivity of pK_{es2} to the nature of the divalent metal indicates that it may be due to a group coordinated to the divalent metal ion, i.e., a coordinated amino acid or possibly the hydroxide bridging both metal ions. In principle, pK_{e2} may originate from a protonation of the free enzyme or the substrate. In the latter case, however, its value should be the same for Fe(III)Fe(II)−BSPAP and Fe(III)Zn(II)−BSPAP, which is not the case. pK_{e2} must, therefore, correspond to a group in the free enzyme that has to be protonated in order for the enzyme to bind substrate. Since pK_{e2} and pK_{es2} are both affected by the metal substitution in a similar way, they may be due to the same active site group, whose pK_a is shifted to lower pH upon substrate binding.

As indicated by their name, all PAPs characterized thus far show optimal activity under mildly acidic conditions. Activity vs pH profiles have been reported for Uf (*36*, *39*), BSPAP (*4*, *11*, *32*), KBPAP (*46*, *47*), and several other mammalian PAPs ((*48*) and references therein) using a variety of substrates and conditions. The pH optima reported range from pH 5.0, typically found for Uf, to pH 6.3 for both FeFe- and FeZn-forms of BSPAP (when assayed at 50 mM *p*-NPP). This is a remarkably large difference, given the fact that Uf and BSPAP are ∼90% homologous and show very similar spectroscopic properties at pH 5.0, suggesting, in turn, similar structural properties at this pH. These apparent discrepancies may be explained (at least partially) by the different conditions used, most importantly substrate concentration, and by the fact that Uf appears to have a substantially lower affinity for *p*-NPP than does BSPAP. We have redetermined the kinetics parameters k_{cat} and K_M for Uf using our standard assay conditions with *p*-NPP as a substrate. We obtained K_M values of 2 and 25 mM at pH 5.0 and 6.0, respectively. These values are ∼10× higher than the corresponding values obtained for BSPAP. Thus, previous studies on the dependence Uf activity on pH were, in hindsight, saturating only for the low pH region. The pH optimum of k_{cat} for Uf is, therefore, predicted to be higher than pH 5.0, and more similar to that of BSPAP.

The pK_a of the acidic limb of the pH optimum was previously determined to be 4.5 for Uf (*36*), 4.8 for BSPAP (*11*), and KBPAP (*47*), which is substantially lower than the pK_a of 5.5 found in this study. One important difference between these studies and the present study has already been mentioned, i.e., the former studies did not determine k_{cat}. A second potential source of error in the previous studies is that the pK_a value was determined graphically by determining the pH at 50% maximal activity. This procedure can lead to misinterpretation of pK_a values when the pK_a values of the acidic and basic limbs are separated by less than 3.5 pH units (*43*), which is clearly the case for the PAPs. Instead, eq 1 must be used to fit the k_{cat} vs pH profile. The results of our kinetics studies suggest that the purple acid phosphatases are not as acidic as normally assumed, especially when k_{cat} is considered.

Structure of Phosphate/Substrate Complex. Both the optical spectra and the EPR spectra of the phosphate complexes of BSPAP show the presence of two forms. The pH titration monitored via optical spectra yields a pK_a of 5.4, which is very similar to that obtained from the k_{cat} vs pH profile. The slightly higher pK_a that is obtained from the pH titration of the EPR spectra may reflect the different temperature at which this pK_a is obtained (freezing point of the buffer solution for EPR vs 22 °C for the activity measurements and the optical spectra).

The EPR spectrum of Fe(III)Fe(II)−BSPAP·PO_4 at pH 5.0 consists of several species. The signal at $g \sim 2.25$ is probably due to the same species that gives rise to the broad and anisotropic spectrum reported previously for Fe(III)Fe(II)−Uf·PO_4. In hindsight, the same signal was also present in the EPR spectrum of Fe(III)Fe(II)−BSPAP·PO_4 reported by Crowder et al. (*13*), although in this report the $g \sim 2.3$ was not discussed and the signals at $g = 1.94$ and 1.75 were ascribed to the Fe(III)Fe(II)−BSPAP·PO_4 complex. The pH titration reported herein showed that the signals at $g = 1.94$ and 1.75 are actually due to a small amount of the high-pH form of the phosphate complex. The signal observed by us at $g = 1.52$ has not been reported previously. One possible explanation for this signal is that our preparations contained a small (∼5%) amount of the molybdate complex (*13*). The pH titration shown in Figure 4 clearly demonstrates that the spectrum represented by the feature at $g = 2.28$ represents the major form at pH 5, while the signals at $g = 1.94$ and 1.73 are due to a small amount of the high-pH form.

Several previous studies have also reported pH-dependent changes in the spectroscopic properties of PAP phosphate complexes. Thus, Dietrich et al. reported pH-dependent changes in the EPR spectra of both free BSPAP and its phosphate complex (*11*). In contrast to their study, however, we do not observe any significant changes in the EPR spectra of the uncomplexed forms of either Fe(III)Fe(II)−BSPAP or Fe(III)Zn(II)−BSPAP from pH 4.5 to 6.5. Also, the changes in the EPR spectra of Fe(III)Fe(II)−BSPAP·PO_4 previously reported (*11*) seem to occur at a lower pH (pK_a 4.6) than those observed by us (p$K_a \sim 6$). In accordance with our present results, these authors reported that λ_{max} shifts to lower wavelengths upon increasing the pH from pH 3.1 to 6.1 (*11*), but again the pK_a obtained in that study (pK_a 4.6) is lower than that found by us (pK_a 5.4). The shape of the EPR spectra of Fe(III)Fe(II)−BSPAP·PO_4 reported by Dietrich et al. (*11*) also differs from those reported for BSPAP in the present study and those reported for Uf at pH 5.0. These discrepancies may be due to the differences in isolation procedure for BSPAP employed (the present study uses the so-called high-salt form of BSPAP (*12*), which is more stable and has a more ordered secondary structure than the low-salt form studied by Dietrich et al. (*11*)). pH-dependent shifts in the absorption maxima (λ_{max}) of the

phosphate complexes of PAPs have been reported in several other studies (*5*, *11*, *12*, *47*). Pyrz et al. observed similar pH-dependent changes in the optical spectra of FeFe−Uf-PO_4 as well as pH-dependent inhibition constants for phosphate, with an apparent pK_a of 5 (*5*). No studies at pH > 6 have been reported for Uf, which may be caused by the fact that the affinity for phosphate becomes rather low at pH > 6.

The structure of the phosphate complex at pH 5.0 has been well studied. EPR studies using $P^{17}O_4$ provided evidence for direct coordination of phosphate to Fe(III) in Fe(III)Zn(II)−Uf (*10*), while EXAFS studies on Fe(III)Zn(II)−Uf·PO_4 revealed a P-scatterer in both the zinc and the iron coordination sphere (*7*). Results of CD and MCD studies on phosphate binding to Uf were also interpreted in terms of a bridging coordination mode for phosphate (*9*). Most convincingly, the X-ray structure of the phosphate complex of KBPAP obtained at pH 4.5 clearly showed a bridging coordination mode for phosphate (*18*). Thus, there exists little doubt that phosphate acts as a bridging ligand to both metal ions at low pH.

The EPR spectrum of Fe(III)Fe(II)−BSPAP·PO_4 at high pH is very similar to that of the uncomplexed protein, both in *g*-values, line widths, and in relaxation properties. This implies that the structure of the diiron center is much less disturbed by phosphate at high pH, which is consistent with binding of phosphate only to the Fe(II). The shift of the tyrosinate-to-Fe(III) charge transfer band to lower wavelengths at higher pH indicates an increase in electron density at the Fe(III), and is also consistent with a model in which the phosphate is replaced by a hydroxide at pH > 5.5. The insensitivity of the FeZn−BSPAP EPR signal to phosphate concentrations up to 30 mM provides the most convincing indication phosphate coordinates only to the divalent metal at pH > 5.5. Although nonbridging coordination of phosphate to only the divalent metal ion provides the simplest explanation for our spectroscopic results at pH 6.5, other coordination modes cannot be excluded.

The use of stopped-flow spectroscopy allowed us to probe for the presence of burst kinetics at pH 7.0, at which PAP still shows 85% of maximal activity. Earlier attempts to detect burst kinetics have been reported both for BSPAP and Uf. Vincent et al. observed burst kinetics for BSPAP at pH 9, but subsequently Wynne et al. failed to observe burst kinetics for Uf at this pH (*32*, *33*). Wynne et al. argued that the burst observed for BSPAP was most likely an experimental artifact. Regardless of the cause of these discrepancies, in both cases the studies were done at a pH at which the enzyme shows less than 1% of its maximum activity. As a result, information obtained under these conditions is unlikely to be directly applicable to the active enzyme.

The major goal of this study was to determine whether the structure of the active enzyme−substrate complex resembles that of the phosphate-bridged form that is known to occur at lower pH. Under steady-state conditions, most of the enzyme will be in the enzyme−substrate-form if the subsequent hydrolysis step is rate-limiting. Our present finding that BSPAP does not display burst kinetics at pH 7.0 means that either the hydrolysis step or a preceding step is rate limiting, rather than release of phosphate. In the case of rate-limiting substrate binding, the samples obtained after the rapid-mixing rapid-freezing experiments should primarily show the EPR spectra of the free enzyme. Instead, these spectra are similar to those of the phosphate complex, both at pH 5 and pH 6.5, providing strong support for the use of phosphate as an analogue of *p*-NPP. Although the spectra are similar, g_x of the Fe(III)Fe(II)−BSPAP·*p*-NPP spectrum at pH 6.5 (1.955) differs significantly from that of Fe(III)-Fe(II)−BSPAP·PO_4 at the same pH (1.944), providing evidence that the enzyme species trapped by this experiment is not the phosphate complex. No significant differences can be detected between the EPR spectra of FeFe−BSPAP-*p*-NPP and FeFe−BSPAP·PO_4 at pH 5.0. We can not presently distinguish between the possibility that the phosphate and *p*-NPP complexes have identical structures and the possibility that release of phosphate is rate-limiting at pH 5.0, so that the enzyme-phosphate complex accumulates at this pH.

Mechanistic Implications. The combination of previous mechanistic and structural studies with the present results allows a more detailed mechanism to be proposed for BSPAP. Mueller et al. have shown that the hydrolysis of the chiral substrate S_p-2′,3′-methoxymethylidene-ATP-$\gamma S\gamma^{18}O\gamma^{17}O$ occurs with overall inversion of the configuration, demonstrating that purple acid phosphatases catalyze the direct hydrolysis of phosphate esters by water, without the formation of a phosphoenzyme intermediate (*35*). Additional support for the absence of a phosphoenzyme intermediate came from the observation that PAPs do not catalyze transphosphorylation reactions (*33*, *34*). Stopped-flow measurements of phosphate binding to Uf suggest a rapid binding of phosphate to Fe^{2+} (*36*, *49*). Our results suggest that, in the catalytically active protonation state, the phosphate ester binds only to the divalent metal. Formation of this enzyme−substrate complex is rapid, since it involves ligand exchange at Fe^{2+} or Zn^{2+}, divalent metal ions that are known to exhibit rapid ligand exchange rates. The simplest explanation for our finding that BSPAP does not show burst kinetics is that the chemical step in catalysis, i.e., attack of water on the phosphate ester, is rate-limiting. If a step after the hydrolysis step were rate-limiting, e.g. release of phosphate, then burst kinetics should have been observed. A second indication that release of phosphate is not rate-limiting comes from our recent finding that the activity of M(III)Zn(II)−BSPAP is relatively insensitive to the nature of the trivalent metal ion (*37*). If release of phosphate were the limiting step in catalysis and involved the breakage of an M(III)-O-bond, k_{cat} values would be predicted to be sensitive to the nature of the trivalent metal ion, which is not the case. The fact that slightly different EPR spectra are obtained after mixing Fe(III)Fe(II)−BSPAP with phosphate and *p*-NPP provides a third argument in favor of the hydrolysis reaction being the rate-limiting step in catalysis rather than phosphate release, since in the latter case the phosphate complex should have accumulated.

A question that has not been answered by this study concerns the nature of the attacking water/hydroxide nucleophile. Three candidates exist: the bridging hydroxide (Scheme 3, mechanism 1), a terminal Fe(III)-coordinated hydroxide (mechanism 2), and a water/hydroxide not directly coordinated to the Fe(III), residing in the second coordination sphere of the metal ion (mechanism 3). Mechanism 1 has been proposed both for Uf (*7*) and for the protein phosphatases PP1 (*29*) and calcineurin (*30*). In this mechanism, the phosphate ester coordinates to both metal ions in a

Scheme 3

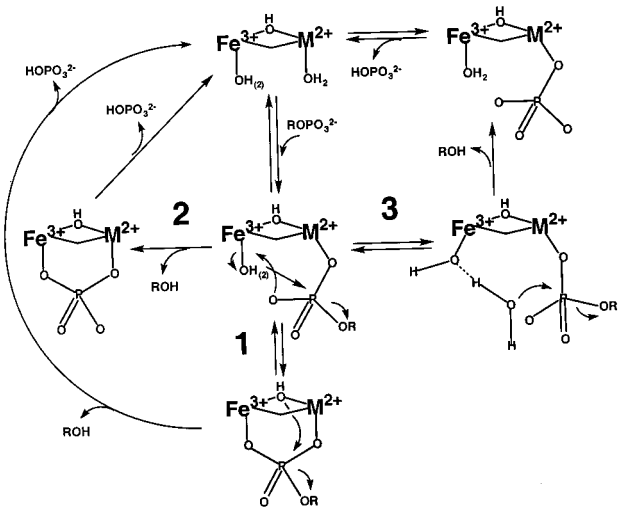

bridging fashion and is then attacked by the bridging hydroxide. At least for the PAPs, the present study suggests that the bridging phosphate complex represents an inactive form of the enzyme−substrate complex.

Witzel and co-workers have argued that the terminal hydroxide on Fe(III) is in a favorable position to attack the phosphate ester if the latter is bound to the divalent metal ion (Scheme 3, mechanism 2) (*11*, *18*). This mechanism requires the formation of a bridging phosphate complex and, therefore, incorporates a step in which ligand exchange (replacement of phosphate by water) must take place at the trivalent metal ion. Since ligand exchange reactions involving trivalent metal ions tend to be slow, the possibility should be considered that such a reaction step may be too slow to be compatible with a turnover rate of ~2000 s^{-1}. Aquino et al. have studied the kinetics of phosphate binding to Uf and reported surprisingly low rate constants, varying from 6.8 s^{-1} (pH 2.7) to 0.42 s^{-1} (pH 6.5) (*36*). Our finding that formation of the bridged phosphate complex at pH 5.0 is nearly complete after 5 ms indicates that this process is faster for BSPAP, but also does not provide information on the rate at which bridge opening occurs. We recently suggested a catalytic mechanism in which an Fe(III)-coordinated hydroxide acts as a general base to deprotonate a water molecule in the second coordination sphere of the Fe(III) (Scheme 3, mechanism 3) (*37*). This hydroxide then attacks the phosphate ester, resulting in a phosphate coordinated only to the divalent metal. In the final step this phosphate is released and another substrate is bound. The attractive feature of this mechanism is that it explains the need for a trivalent metal ion (generation of a hydroxide complex that acts as a general base), without the need to postulate a ligand exchange reaction at the trivalent metal.

Distinguishing between the mechanistic possibilities mentioned above may not be trivial. The following paper in this issue describes the inhibition by and coordination chemistry of fluoride with BSPAP. Since fluoride can be considered to be a structural analogue of hydroxide, the structure of the fluoride complex is expected to reveal more about the nature of the hydroxide that participates in catalysis. The present work indicates that the structure of the phosphate complex at pH 6.5 corresponds to the structure of the catalytically active enzyme−substrate complex. Whether our structural model for the phosphate−substrate complex at this pH is correct remains to be verified by subsequent spectroscopic and structural studies using techniques such as X-ray diffraction, EXAFS, and ENDOR/ESEEM.

ACKNOWLEDGMENT

We thank Raymond Ho and Prof. L. Que Jr. for supplying us with a sample of uteroferrin, Brendan Quirk for his initial experiments on the pH optima of BSPAP, Henk Dekker for assistance with stopped-flow optical spectroscopy, Winfried Roseboom for assistance with the rapid-freeze experiments, and Rico Funhoff for critically reading the manuscript. This research was supported in part by the EC Biotechnology Program.

SUPPORTING INFORMATION AVAILABLE

EPR spectra of FeZn−BSPAP at pH 6.5 in the presence of various, high concentrations of phosphate including a plot of the signal intensity at $g = 4.3$ as a function of phosphate concentration (Figure S1). This material is available free of charge via the Internet at http://pubs.acs.org.

REFERENCES

1. Sträter, N., Lipscomb, W. N., Klabunde, T., and Krebs, B. (1996) *Angew. Chem., Int. Ed. 35*, 2024−2055.
2. Wilcox, D. E. (1996) *Chem. Rev. 96*, 2435−2458.
3. Klabunde, T., and Krebs, B. (1997) *Structure and Bonding 89*, 177−198.
4. Merkx, M., and Averill, B. A. (1998) *Biochemistry 37*, 11223−11231.
5. Pyrz, J. W., Sage, J. T., Debrunner, P. G., and Que, L., Jr. (1986) *J. Biol. Chem. 261*, 11015−11020.
6. Wang, X., and Que, L., Jr. (1998) *Biochemistry 37*, 7813−7821.
7. Wang, X., Randall, C. R., True, A. E., and Que, L., Jr. (1996) *Biochemistry 35*, 13946−13954.
8. Day, E. P., David, S. S., Peterson, J., Dunham, W. R., Bonvoison, J. J., Sands, R. H., and Que, L., Jr. (1988) *J. Biol. Chem. 263*, 15561−15567.
9. Yang, Y. S., McCormick, J. M., and Solomon, E. I. (1997) *J. Am. Chem. Soc. 119*, 11832−11842.
10. David, S. S., and Que, L., Jr. (1990) *J. Am. Chem. Soc. 112*, 6455−6463.
11. Dietrich, M., Münstermann, D., Suerbaum, H., and Witzel, H. (1991) *Eur. J. Biochem. 199*, 105−113.
12. Vincent, J. B., Crowder, M. W., and Averill, B. A. (1991) *Biochemistry 30*, 3025−3034.
13. Crowder, M. W., Vincent, J. B., and Averill, B. A. (1992) *Biochemistry 31*, 9603−9608.
14. Crans, D. C., Simone, C. M., Holz, R. C., and Que, L., Jr. (1992) *Biochemistry 31*, 11731−11739.
15. True, A. E., Scarrow, R. C., Randall, C. R., Holz, R. C., and Que, L., Jr. (1993) *J. Am. Chem. Soc. 115*, 4246−4255.
16. Scarrow, R. C., Pyrz, J. W., and Que, L., Jr. (1990) *J. Am. Chem. Soc. 112*, 657−665.
17. Sträter, N., Klabunde, T., Tucker, P., Witzel, H., and Krebs, B. (1995) *Science 268*, 1489−1492.
18. Klabunde, T., Sträter, N., Fröhlich, R., Witzel, H., and Krebs, B. (1996) *J. Mol. Biol. 259*, 737−748.
19. Klabunde, T., Sträter, N., Krebs, B., and Witzel, H. (1995) *FEBS Lett. 367*, 56−60.
20. Davis, J. C., and Averill, B. A. (1982) *Proc. Natl. Acad. Sci. U.S.A. 79*, 4623−4627.
21. Beck, J. L., Keough, D. T., de Jersey, J., and Zerner, B. (1984) *Biochim. Biophys. Acta 791*, 357−363.
22. Merkx, M., and Averill, B. A. (1998) *Biochemistry 37*, 8490−8497.
23. Beck, J. L., de Jersey, J., Zerner, B., Hendrich, M. P., and Debrunner, P. G. (1988) *J. Am. Chem. Soc. 110*, 3317−3318.

24. Beck, J. L., McArthur, M. J., de Jersey, J., and Zerner, B. (1988) *Inorg. Chim. Acta 153*, 39−44.
25. Suerbaum, H., Körner, M., Witzel, H., Althaus, E., Mosel, B.-D., and Müller-Warmuth, W. (1993) *Eur. J. Biochem. 214*, 313−321.
26. Koonin, E. V. (1994) *Protein Sci. 3*, 356−368.
27. Zhuo, S., Clemens, J. C., Stones, R. L., and Dixon, J. E. (1994) *J. Biol. Chem. 269*, 26234−26238.
28. Goldberg, J., Huang, H.-B., Kwon, Y.-G., Greengard, P., Nairn, A. C., and Kuriyan, J. (1995) *Nature 376*, 745−753.
29. Egloff, M. P., Cohen, P. T. W., Reinemer, P., and Barford, D. (1995) *J. Mol. Biol. 254*, 942−959.
30. Griffith, J. P., Kim, J. L., Kim, E. E., Sintchak, M. D., Thomson, J. A., Fitzgibbon, M. J., Fleming, M. A., Caron, P. R., Hsiao, K., and Navia, M. A. (1995) *Cell 82*, 507−522.
31. Kissinger, C. R., Parge, H. E., Knighton, D. R., Lewis, C. T., Pelletier, L. A., Tempczyk, A., Kalish, V. J., Tucker, K. D., Showalter, R. E., Moomaw, E. W., Gastinel, L. N., Habuka, N., Chen, X., Maldonado, F., Barker, J. E., Bacquet, R., and Villafranca, J. E. (1995) *Nature 378*, 641−644.
32. Vincent, J. B., Crowder, M. W., and Averill, B. A. (1991) *J. Biol. Chem. 266*, 17737−17740.
33. Wynne, C. J., Hamilton, S. E., Dionysius, D. A., Beck, J. L., and de Jersey, J. (1995) *Arch. Biochem. Biophys. 319*, 133−141.
34. Quirk, B. J. (1995) *Ph.D. Thesis* University of Virginia, USA.
35. Mueller, E. G., Crowder, M. W., Averill, B. A., and Knowles, J. R. (1993) *J. Am. Chem. Soc. 115*, 2974−2975.
36. Aquino, M. A. S., Lim, J.-S., and Sykes, A. G. (1994) *J. Chem. Soc., Dalton Trans.* 429−436.
37. Merkx, M., and Averill, B. A. (1999) *J. Am. Chem. Soc. 121*, 6683−6689.
38. Keough, D. T., Beck, J. L., de Jersey, J., and Zerner, B. (1982) *Biochem. Biophys. Res. Commun. 108*, 1643−1648.
39. Schlosnagle, D. C., Blazer, F. W., Tsibris, J. C. M., and Roberts, R. M. (1974) *J. Biol. Chem. 249*, 7574−7579.
40. Aasa, R., and Vänngård, T. (1975) *J. Magn. Res. 19*, 308−315.
41. Albracht, S. P. J. (1984) *Current Topics in Bioenergetics 13*, 79−106.
42. de Vries, S., Albracht, S. P. J., Berden, J. A., and Slater, E. C. (1982) *Biochim. Biophys. Acta 681*, 41−53.
43. Segel, I. H., *Enzyme Kinetics: Behaviour and analysis of rapid equilibrium and steady-state enzyme systems*, 1993, New York: John Wiley & Sons.
44. Davis, J. C., Lin, S. S., and Averill, B. A. (1981) *Biochemistry 20*, 4062−4067.
45. Fersht, A., *Enzyme structure and mechanism*, 2nd ed., 1985, New York: W. H. Freeman.
46. Cashikar, A. G., Kumaresan, R., and Rao, N. M. (1997) *Plant Physiology 114*, 907−915.
47. Körner, M. (1992) *Ph.D. Thesis* University of Münster, Germany.
48. Vincent, J. B., and Averill, B. A. (1990) *FASEB 4*, 3009−3014.
49. Aquino, M. A. S., Lim, J.-S., and Sykes, A. G. (1992) *J. Chem. Soc., Dalton Trans.* 2135−2136.

BI9904454